2019 EAGE ANNUAL
81ST CONFERENCE + EXHIBITION
LONDON | THE UNITED KINGDOM

Th_R08_06

Multiparameter FWI of 3D OBC Dataset From the Valhall Field

N. Kamath[1]*, R. Brossier[1], L. Metivier[1], P. Yang[2]

[1] University of Grenoble Alps; [2] Electromagnetic Geoservices ASA

Summary

Full-waveform inversion (FWI) performed in areas with known attenuation can yield distorted velocities when viscous effects are not taken into account. Monoparameter (velocity-only) visco-acoustic FWI using a crude attenuation (Qp) model can improve the estimated velocity. However, joint inversion to update both velocity and attenuation is ideal, as the obtained Qp can be used for migrating the data. We invert the pressure component of ocean bottom cable (OBC) data acquired in the Valhall field for P-wave vertical velocity VP0 and attenuation Qp . A data subsampling strategy is employed to ensure efficient use of computational resources. Simultaneous inversion of VP0 and Qp results in velocities larger than when the medium is considered acoustic. However, the difference in the velocities obtained from joint inversion and monoparameter visco-acoustic inversion is not significant.

Introduction

Multiparameter full-waveform inversion (FWI) is a challenging problem because of the inherent trade-offs between the different model parameters (Virieux and Operto, 2009; Virieux et al., 2017). Choosing a suitable parameterization for the inversion by analysing radiation patterns can help mitigate the problem (Kamath et al., 2017). In viscous media, although velocity and the attenuation Q_p scatter the wavefield equally in all directions (Yang et al., 2018), the $\pi/2$ phase-shift introduced by Q_p should help resolve the two parameters (Hak and Mulder, 2011). It is, however, still necessary to choose an inversion algorithm with an appropriate preconditioner to ensure meaningful parameter updates.

Operto and Miniussi (2018) perform frequency-domain FWI of 3D ocean bottom cable (OBC) data from the Valhall field, which exhibits VTI (transverse isotropy with a vertical symmetry axis) symmetry and significant attenuation. They invert for P-wave vertical velocity V_{P0}, density ρ and attenuation and conclude that the estimated velocity and Q_p are more reliable than ρ. Wang et al. (2018) invert data from the North Sea for velocity and attenuation simultaneously. The Q-compensated migration images generated from these parameters have consistent amplitudes and better-resolved events.

In this study, we invert Ocean Bottom Cables (OBC) data from the Valhall field, different from those from Operto and Miniussi (2018). Only the pressure data are taken into account and both velocity-only and multiparameter (V_{P0} and Q_p) updates are performed.

Model and data

The Valhall field is characterized by a chalk reservoir at a depth of 2.5 km and is overlain by a gas cloud (Barkved et al., 2010), which makes imaging beneath it challenging. The medium is anisotropic (VTI), with ε and δ reaching values of up to 0.2 and 0.08, respectively. The height of the water column is almost constant at 70 m (shallow water environment). The initial models for V_{P0} and ε, obtained through conventional tomography, and δ, from well-ties, were provided to us by AkerBP. We build the density-field from V_{P0} using a standard Gardner's relationship.

The multicomponent OBC data were acquired by AkerBP in 2011. The survey covers an area of approximately 145 square km and a total of 50,824 shots, at a depth of 5 m, generate the data. Thirteen cables, 300 m apart, and containing 2048 receivers, were used to record the wavefield. Both the shot- and receiver-spacing are 50 m. The data given to us had no pre-processing applied and hence we perform the following steps: rotate and translate the data to the computation grid, apply source-receiver reciprocity, remove spiky traces, and apply minimum-phase filter to divide the data into two sets of frequency bands ($2.5-5$ Hz and $2.5-7$ Hz). Only the hydrophone component is employed in the inversion.

Inversion

Time-domain finite-difference modelling (4th order in space and 2nd order in time) is used to generate acoustic wavefield in VTI media (Duveneck and Bakker, 2011). In the presence of attenuation, three standard linear solid (SLS) mechanisms (Yang et al., 2018) are employed to compute the wavefield. We use the checkpoint-assisted reverse forward simulation (CARFS) technique to obtain the gradient of the objective function with respect to the model parameters (Yang et al., 2016).

The preconditioned *l*-BFGS algorithm implemented in the SEISCOPE optimization toolbox (Métivier and Brossier, 2016) updates the model every iteration. Depth preconditioning involves weighting the gradient by a function of depth ($z^{1.5}$, z being the depth) to compensate for amplitude decay from geometrical spreading. Yang et al. (2018) showed, for a synthetic 2D model, that a pseudo-Hessian preconditioner, computed by weighting the source wavefield by the scattering matrix can better account for the tradeoffs between different model parameters.

In order to ensure that we take all the data into account without sacrificing computational efficiency, we use a data subsampling strategy (Kamath et al., 2018). The dataset are divided into sixteen groups of 128

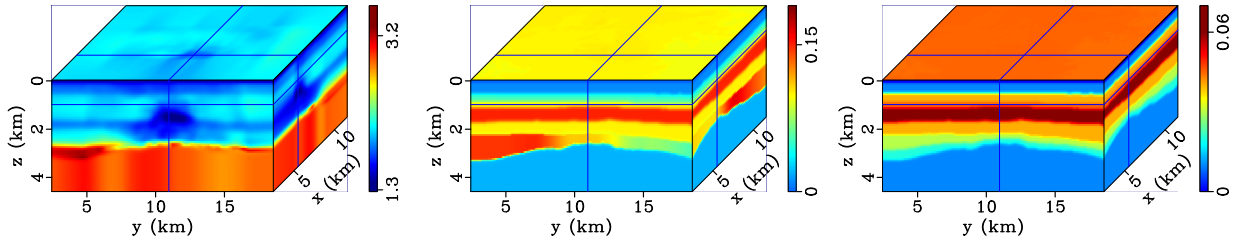

(a) (b) (c)

Figure 1: Initial (a) P-wave vertical velocity V_{P0}, and the anisotropy coefficients (b) ε and (c) δ.

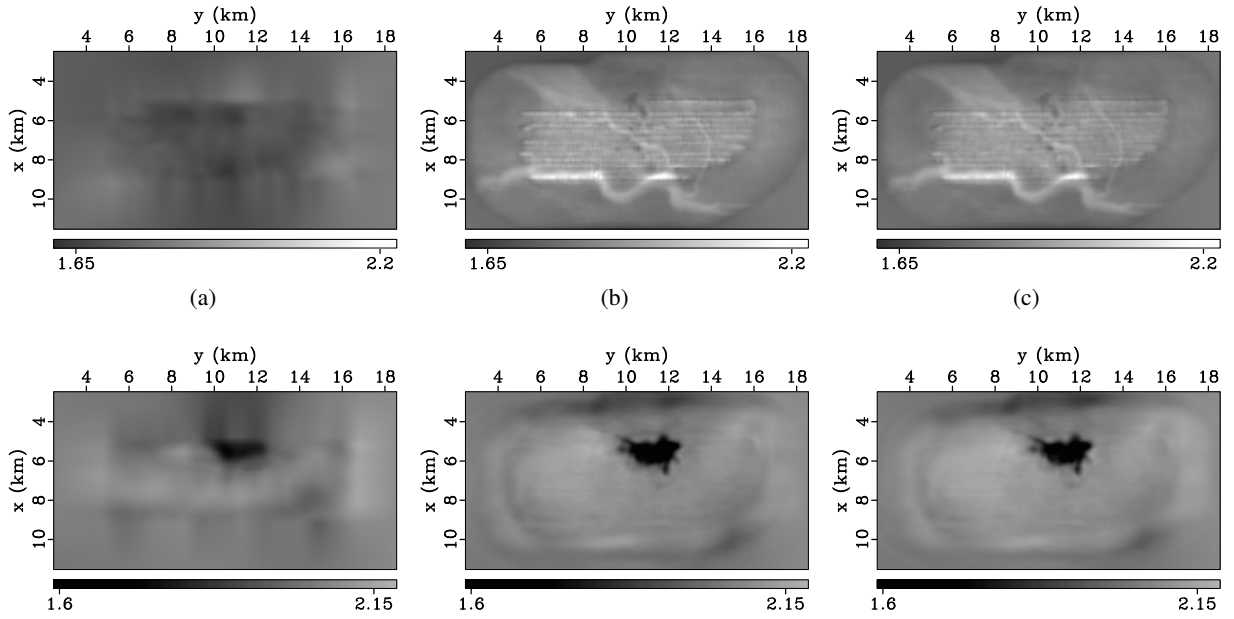

(a) (b) (c)

(d) (e) (f)

Figure 2: (a) Initial P-wave vertical velocity V_{P0} at a depth of 200 m. The V_{P0} at the same depth obtained after FWI (b) without attenuation, and (c) in viscous media. The (d) initial V_{P0} at a depth of 1000 m, inversion results (e) in the absence and (f) in the presence of attenuation. The units of velocity here, and in the following figures are km/s.

randomly selected shots, with no repetition in shots. Three iterations of l-BFGS are run on each group, with the resulting output serving as the input for the next group. The entire procedure is performed two times so that each shot gather is used twice during the entire inversion. The total number of l-BFGS iterations thus reaches 96. The density- and anisotropy-fields remain unchanged during inversion.

Results

Starting from the initial model (Figure 1), the same number of iterations of FWI are run without (Figures 2b and 2e) and with (Figures 2c and 2f) attenuation taken into account. For the latter case, a Q_p model is built such that its values are 1000 in the water column, 100 in the sediments where $V_{P0} < 1600$ m/s, and 200 elsewhere. Both acoustic and visco-acoustic FWI manage to update the velocities in the shallow region ($z = 200$m) significantly: the underground channels are clearly visible. Although acoustic FWI yields an improved V_{P0}, the gas cloud is better resolved when $Q_p \neq 0$ (compare Figures 2e and 2f). Note that in the presence of attenuation, the stiffness coefficients (and, hence, the velocity) become frequency dependent. In our implementation of the SLS mechanisms, the inverted V_{P0} corresponds to the unrelaxed modulii, i.e., the ones at infinite frequencies. Hence, the mean P-wave vertical velocity is higher (by 1.2% at $z = 1000$ m, although locally, the values can be as high as 9%) when the medium is considered viscous.

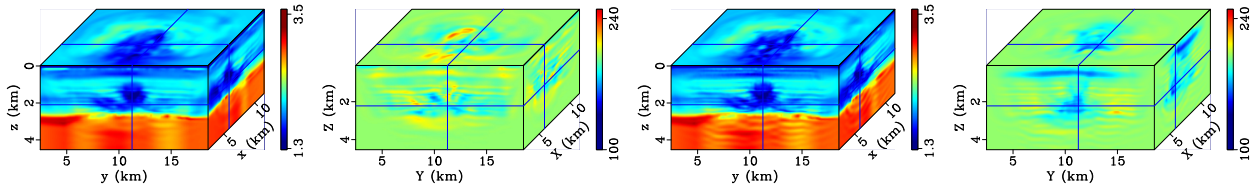

(a) (b) (c) (d)

Figure 3: Joint inversion of velocity and attenuation: (a) P-wave vertical velocity V_{P0} and (b) attenuation Q_p obtained using pseudo-Hessian preconditioner. The inverted (c) V_{P0} and (d) Q_p from depth-preconditioning.

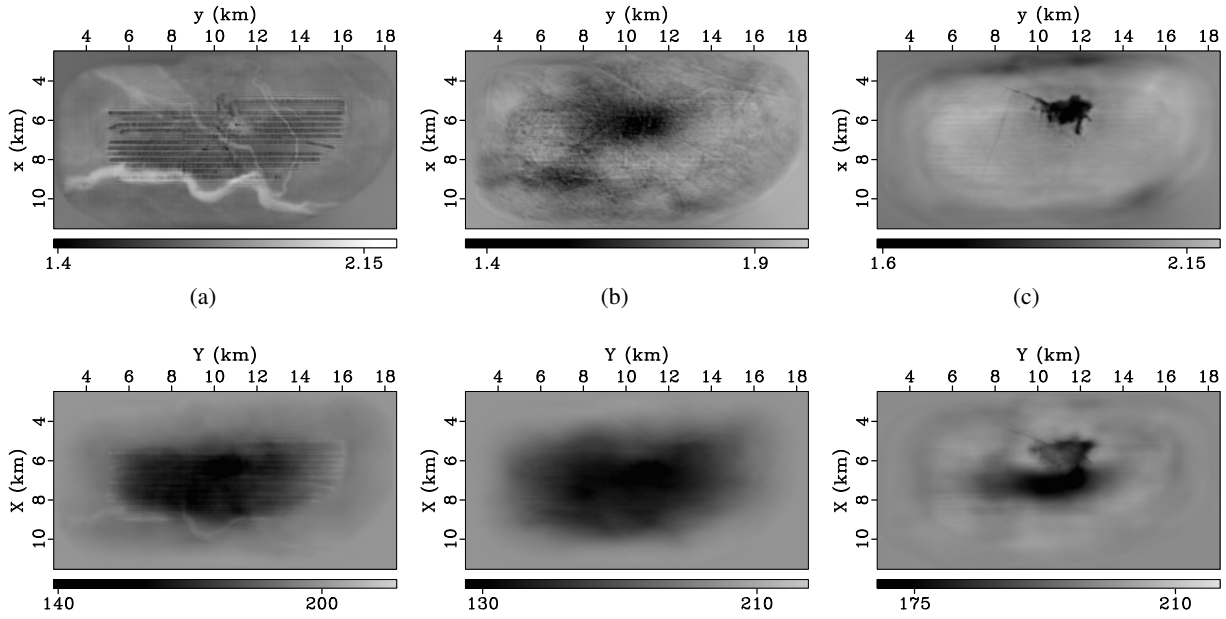

(a) (b) (c)

(d) (e) (f)

Figure 4: Velocities at (a) $z = 200$ m, (b) $z = 500$ m, and (c) $z = 1000$ m obtained from joint inversion of V_{P0} and Q_p using depth-preconditioning, for frequencies in the data up to 7 Hz. The inverted attenuation Q_p at depths of (d) 200 m, (e) 500 m, and (f) 1000 m.

The above results demonstrate the importance of an accurate Q_p model. Starting from the same initial V_{P0} model as before and a constant Q_p-field (values of 1000 in the water column and 200 in the sediments), we simultaneously invert for V_{P0} and Q_p. Both parameters are normalized in the optimization so that their values lie between 0 and 1. While the depth preconditioner does not require any tuning, the pseudo-Hessian preconditioner has three parameters that must be tested: a scaling which controls the magnitude of updates in each parameter relative to the other; and damping coefficients, which control the values as a function of depth within each parameter.

Using the pseudo-Hessian preconditioner, however, the reconstruction of the attenuation model seems less satisfactory (compare Figures 3b and 3d), most likely because of the sparseness of the shots. In addition, the preconditioner is very sensitive to the damping coefficients, which balance the amplitudes of the gradient as a function of depth. Because of the decoupling the pseudo-Hessian is supposed to provide between the different model parameters, the effort in finding appropriate coefficients could prove beneficial.

Next, we invert data that contain frequencies of up to 7 Hz for velocity-only visco-acoustic FWI, and joint ($V_{P0} - Q_p$) updates using depth preconditioning. We notice a correlation between the low velocities and the lower values of Q_p in the inverted results (Figure 4), although at $z = 1000$ m (Figure 4f), there seem to be some artefacts in the obtained Q_p. It is interesting to note that at $z = 1000$ m, the difference between the V_{P0} from the joint inversion (Figure 4c) and that obtained from the mono-parameter visco-

acoustic inversion (not shown here) is less than 0.05%. It remains to be seen if a fixed Q_p model will suffice as we include higher frequencies, where the influence of attenuation is larger.

Ongoing work and conclusions

In the frame of mono-parameter (velocity-only) FWI of this 3D OBC dataset from the Valhall field, even for frequencies ranging from $2.5-5$ Hz, taking attenuation into account improves the resolution of the estimated V_{P0}-model. Simultaneous inversion of P-wave vertical velocity V_{P0} and attenuation Q_p using a depth-preconditioned l-BFGS algorithm results in Q_p-updates which correlate with lower velocities in the sediments. We note, however, the presence of some Q_p artefacts up shallow (for $0.5 < z < 1$ km). An appropriate pseudo-Hessian preconditioner, less sensitive to sparse shot-sampling, could help reduce these artefacts during joint inversion, and is worth investigating.

For the frequencies used here, V_{P0}-only inversion with a crude background Q_p model yields updates very similar to the joint inversion. At higher frequencies, however, the larger influence of attenuation ought to result in larger differences in the estimated V_{P0}. The next step will be to further incorporate higher frequencies for joint inversion and migrate data to QC the results.

Acknowledgements

This study was partially funded by the SEISCOPE consortium (*http://seiscope2.osug.fr*), sponsored by AKERBP, CGG, CHEVRON, EQUINOR, EXXON-MOBIL, JGI, PETROBRAS, SCHLUMBERGER, SHELL, SINOPEC and TOTAL. This study was granted access to the HPC resources of CIMENT infrastructure (https://ciment.ujf-grenoble.fr) and CINES/IDRIS/TGCC under the allocation 046091 made by GENCI. We thank AKERBP ASA and their partner Pandion Energy for providing the dataset and permission to present this work, and the help of Ross Milne from AKERBP.

References

Barkved, O., Heavey, P., Kommedal, J.H., van Gestel, J.P., ve, R.S., Pettersen, H., Kent, C. and Albertin, U. [2010] Business Impact of Full Waveform Inversion at Valhall. SEG Technical Program Expanded Abstracts, **29**(1), 925–929.

Duveneck, E. and Bakker, P.M. [2011] Stable P-wave modeling for reverse-time migration in tilted TI media. Geophysics, **76**(2), S65–S75.

Hak, B. and Mulder, W.A. [2011] Seismic attenuation imaging with causality. Geophysical Journal International, **184**(1), 439–451.

Kamath, N., Brossier, R., Métivier, L. and Yang, P. [2018] 3D acoustic/viscoacoustic time-domain FWI of OBC data from the Valhall field. In: SEG Technical Program Expanded Abstracts 2018. 1093–1097.

Kamath, N., Tsvankin, I. and Díaz, E. [2017] Elastic full-waveform inversion for VTI media: A synthetic parameterization study. Geophysics, **82(5)**, C163–C174.

Métivier, L. and Brossier, R. [2016] The SEISCOPE Optimization Toolbox: A large-scale nonlinear optimization library based on reverse communication. Geophysics, **81**(2), F11–F25.

Operto, S. and Miniussi, A. [2018] On the role of density and attenuation in 3D multi-parameter visco-acoustic VTI frequency-domain FWI: an OBC case study from the North Sea. Geophysical Journal International, **213**, 2037–2059.

Virieux, J., Asnaashari, A., Brossier, R., Métivier, L., Ribodetti, A. and Zhou, W. [2017] An introduction to Full Waveform Inversion. In: Grechka, V. and Wapenaar, K. (Eds.) Encyclopedia of Exploration Geophysics, Society of Exploration Geophysics, R1–1–R1–40.

Virieux, J. and Operto, S. [2009] An overview of full waveform inversion in exploration geophysics. Geophysics, **74**(6), WCC1–WCC26.

Wang, M., Xie, Y., Xiao, B., Ratcliffe, A. and Latter, T. [2018] Visco-acoustic full-waveform inversion in the presence of complex gas clouds. In: SEG Technical Program Expanded Abstracts 2018. 5516–5520.

Yang, P., Brossier, R., Métivier, L. and Virieux, J. [2016] Wavefield reconstruction in attenuating media: A Checkpointing-assisted reverse-forward simulation method. Geophysics, **81**(6), R349–R362.

Yang, P., Brossier, R., Métivier, L., Virieux, J. and Zhou, W. [2018] A Time-Domain Preconditioned Truncated Newton Approach to Multiparameter Visco-acoustic Full Waveform Inversion. SIAM Journal on Scientific Computing, **40**(4), B1101–B1130.